THE ASTROPHYSICAL JOURNAL, 205:638–654, 1976 April 15

PHOTONUCLEAR INTERACTIONS OF ULTRAHIGH ENERGY COSMIC RAYS AND THEIR ASTROPHYSICAL CONSEQUENCES

J. L. PUGET,* F. W. STECKER, AND J. H. BREDEKAMP
Theoretical Studies Group, NASA Goddard Space Flight Center
Received 1975 June 30; revised 1975 September 24

ABSTRACT

We present here the results of detailed Monte Carlo calculations of the interaction histories of ultrahigh energy cosmic-ray nuclei with intergalactic radiation fields using improved estimates of these fields and empirical determinations of photonuclear cross sections including multinuclear disintegrations for nuclei up to ^{56}Fe. Intergalactic and galactic energy loss rates and nucleon loss rates for nuclei up to ^{56}Fe are also given. Astrophysical implications are discussed in terms of expected features in the cosmic-ray spectrum between 10^{18} and 10^{21} eV for the universal and supercluster origin hypotheses. The results of these calculations indicate that *ultrahigh energy cosmic rays cannot be universal in origin regardless of whether they are protons or nuclei.* Both the supercluster and galactic origin hypotheses, however, are possible regardless of nuclear composition.

Subject headings: cosmic rays: abundances — cosmic rays: general — nuclear reactions

I. INTRODUCTION

The basic interactions between photons and nuclei of ultrahigh energy which have important astrophysical consequences are the following: (1) Compton interactions, (2) pair production (particularly of e^+e^- pairs) in the field of the nucleus, (3) photodisintegration of the nucleus, and (4) photoproduction of hadrons.

In the rest-system of the nucleus, process (1) has no threshold energy, process (2) occurs at a threshold energy of $2m_ec^2 \approx 1$ MeV, process (3) is particularly important in most cases between 15 and 25 MeV where the giant dipole resonance has its peak, and process (4) has a threshold energy of

$$\varepsilon_{\text{th}}' = m_\pi c^2(1 + m_\pi/2m_p) \approx 145 \quad \text{MeV} . \tag{1}$$

Process (1), Compton effect interactions involving nuclei, is a process which results in only a negligibly small energy loss for the nuclei given by

$$-\frac{dE}{dt} = \frac{4}{3}\rho_\gamma\sigma_T c\left(\frac{m_e}{Am_p}\right)^2 Z^4\left(\frac{E}{Am_pc^2}\right)^2 = \frac{Z^4}{A^2}\rho_\gamma\left(\frac{E}{Am_pc^2}\right)^2 \text{eV s}^{-1} , \tag{2}$$

where ρ_γ is the energy density of the ambient photon field in eV cm^{-3}, σ_T is the Thomson cross section, and Z and A are the atomic number and weight of the nucleus with E being the total energy of the nucleus in eV.

Processes (2) through (4) must be considered in investigating the propagation ultrahigh energy cosmic-ray nuclei in intergalactic space (Greisen 1966; Zatsepin and Kuz'min 1966; Stecker 1968, 1969; Berezinskii and Zatsepin 1971).

Process (2), pair-production, particularly important for heavy nuclei, has been treated in detail in its astrophysical context by Blumenthal (1970). This process is only of importance for interactions with the 2.7 K blackbody background radiation (see § IV). In this case, for interactions with a blackbody field of temperature T, the photon density is given by the Planck function

$$n(\epsilon) = (\hbar c)^{-3}(\epsilon/\pi)^2(e^{\epsilon/kT} - 1)^{-1} , \tag{3}$$

and the energy loss rate for the nucleus is

$$-(dE/dt) = 3\alpha\sigma_T h^{-3}Z^2(m_ec^2kT)^2 f[m_ec^2/(2\gamma kT)] , \tag{4}$$

where $f(\nu)$ is shown in Figure 1. The Lorentz factor of the nucleus $\gamma = E(Am_pc^2)^{-1}$.

The photohadron production process (4) is dominated by photopion production channels. This process has been treated in detail in a previous paper (Stecker 1968). Figure 2 shows the lifetime and mean free path for protons against attenuation by energy loss due to pair production (Blumenthal 1970) and photomeson production (Stecker

* NAS/NRC Postdoctoral Resident Research Associate.

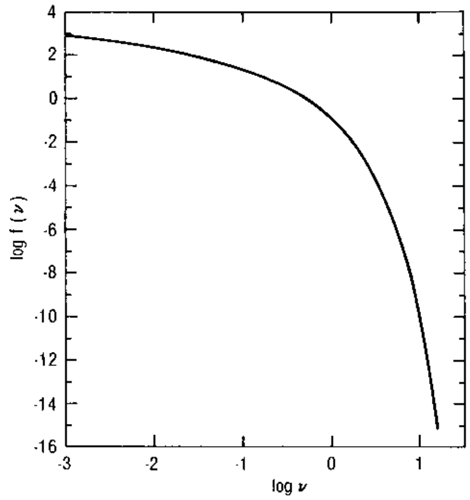

FIG. 1.—A graph of the function $f(\nu)$ used in eq. (4) as defined by Blumenthal (1970)

1968) due to interactions with the 2.7 K radiation. Also shown in Figure 2 is the lifetime for ^{56}Fe against energy loss by e^+e^- pair production.

Process (3), photodisintegration, is not as easy to treat as the other processes and most previous cosmic-ray papers have used only simple estimates of the cross section for this process. Stecker (1969) used a detailed study of ^{4}He photodisintegration (Gorbunov 1968) to determine the lifetime of ^{4}He and estimate the lifetime of ^{56}Fe against one nucleon loss by interactions with the 2.7 K radiation. The main emphasis in this paper will be on a presentation of the results of a new and much more detailed calculation of the intergalactic photodisintegration of ultrahigh energy nuclei with the following improvements:

1. Use of empirically determined cross section data as a function of energy for all nuclei with $1 \leq A \leq 56$. Because of the position of ^{56}Fe on the binding energy curve, it is considered to be a significant end product of stellar evolution, and higher mass nuclei are found to be much rarer in the cosmic radiation.

2. Use of cross section data for $1 \leq A \leq 57$ for *multinucleon emission* interactions as well as single nucleon emission interactions. Multinucleon losses (except for double nucleon loss) involve nonresonant processes and are

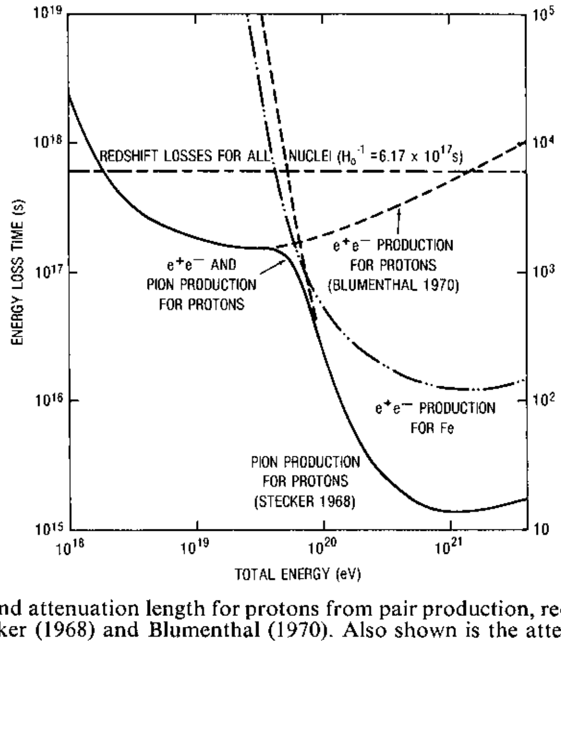

FIG. 2.—The energy loss time and attenuation length for protons from pair production, redshift, and photopion production losses based on the calculations of Stecker (1968) and Blumenthal (1970). Also shown is the attenuation length for ^{56}Fe from pair production losses.

particularly important at energies between the position of the giant dipole resonance and the pion production threshold (i.e., 25 MeV $< \epsilon' <$ 145 MeV; see § II).

3. Use of new estimates of the intergalactic infrared radiation field, whose effect is included along with that of the blackbody radiation.

4. Inclusion of energy loss by pair production occurring concurrently with energy loss by photodisintegration.

5. Treatment of these concurrent energy loss processes by using numerical Monte Carlo techniques which also allow a natural treatment of the multinucleon loss processes in a determination of the photodisintegration and energy loss histories of nuclei as a function of initial energy.

II. PHOTODISINTEGRATION PROCESS

A general discussion of the photonuclear interaction process for the energies of interest here has been given by Danos and Fuller (1965) and Hayward (1970). This energy band, extending up to 150 MeV, or about the meson production threshold, rather naturally splits into two parts. The lower region, extending up to 30 MeV, has been studied extensively. This is the domain of the giant resonances of the nuclear photoeffect. Here, although two-nucleon emission does take place, most of the absorption cross section results in the emission of only single nucleons, either neutrons or protons. For the medium and heavy nuclei, $A \geq 50$, the total photon absorption cross section can be well represented by a single, or in the case of the deformed nuclei, by the superposition of two Lorentzian curves of the form

$$\sigma(\epsilon') = \sigma_0 \frac{\epsilon'^2 \Gamma_d{}^2}{(\epsilon'_0{}^2 - \epsilon'^2)^2 + \epsilon'^2 \Gamma_d{}^2} . \tag{5}$$

For the lighter nuclei, the absorption cross section often shows considerably more structure than this. For all nuclei the basic photonuclear interaction at these energies is pictured as being with the individual uncorrelated nucleons comprising the nucleus. In the shell model language, the interaction results in the creation of particle-hole pairs. The collective giant resonance state is described by a coherent superposition of individual single-particle transitions.

The data for energies between 30 and 150 MeV are relatively sparse. The available measurements seem to indicate that the total cross section in this region is a relatively smooth function of energy. Reactions in which a number of nucleons are emitted seem to make up most of the total absorption cross section. In this region the photon's wavelength becomes comparable with, and less than, nuclear dimensions, and it becomes very difficult to conserve both energy and momentum in a single-particle interaction within the nucleus. The dominant absorption process is then pictured as one in which the photon interacts with a nucleon pair while they are scattering within the nucleus. This is referred to as the quasi-deuteron effect (Levinger 1951).

In the following discussion, the strength of a photonuclear reaction in the two energy regions, i.e., the integral of the cross section over the energy interval, will be given in units of the classical dipole sum rule, i.e.,

$$\sum_d = \int \sigma(\epsilon') d\epsilon' = \frac{2\pi^2 e^2}{Mc} \frac{NZ}{A} = 59.8 \frac{NZ}{A} \quad \text{MeV-mb} , \tag{6}$$

where M is the nucleon mass, A the mass number, Z the number of protons, and N the number of neutrons in the nucleus. The derivation of this result is based both on the long wavelength approximation for the dipole operator involving nucleon coordinates only and on closure, i.e., it assumes that the integration in equation (6) is carried out over all excitation energies. Meson coordinates within nuclei are specifically ignored. Since these assumptions are not valid for the excitations being considered here, no real physical significance should be attached to this normalization. It is simply a convenient scale factor that removes the *principal* dependence of the total absorption cross section on N, Z, and A.

The data used in these calculations were based on an evaluation of the information in the files of the Photonuclear Data Center at the National Bureau of Standards (E. G. Fuller, private communication). To simplify these calculations, the observed detailed dependence of the various reaction cross sections on photon energy was not used. Rather, each cross section was assumed to be independent of energy over a finite energy band of width Δ. For energies below 30 MeV, this band is assumed to be centered about a mean energy ϵ_0' for each reaction. As a further simplification, it was assumed that the half-lives of the various reaction products resulting from photonuclear reactions were all short compared with the rate at which the reactions take place. With this assumption, it was not necessary to consider each individual reaction; only the cross section for emitting ΔA nucleons from a nucleus of mass A had to be input into the calculations.

The data used in the calculations are given in Tables 1 and 2. For energies below 30 MeV, the total absorption cross section is assumed to result in reactions in which only one or two nucleons are emitted. These are given in terms of the quantities ϵ_0', ξ, and Δ listed in Table 1 with the subscripts 1 or 2, respectively. For each reaction, these were defined as follows:

$$\xi_1 = \frac{1}{\sum_d} \int_0^{30} \sigma^{(1)}(\epsilon') d\epsilon' , \tag{7}$$

where $\sigma^{(1)}(\epsilon')$ is the actual single nucleon emission cross section as a function of photon energy ϵ'.

TABLE 1

Cross Section Parameters for Photonuclear Emission Processes (ϵ and Δ in MeV)

A	$\epsilon_{0,1}'$	ξ_1	Δ_1	$\epsilon_{0,2}'$	ξ_2	Δ_2	ζ	Element
56.........	18	0.98	8	22	0.15	7	0.95	Fe
55.........	18	0.93	7	23.5	0.20	8	0.95	Mn
54.........	18	0.93	7	24	0.20	8	0.95	Cr
53.........	18	1.03	7	24	0.10	8	0.95	Cr
52.........	18	1.08	7	24	0.05	8	0.95	Cr
51.........	19	1.02	7	25	0.11	6	0.95	V
50.........	19	1.03	8	25	0.10	6	0.95	Ti
49.........	19	1.03	8	25	0.10	6	0.95	Ti
48.........	19	1.03	8	25	0.10	6	0.95	Ti
47.........	19	1.03	8	25	0.10	6	0.95	Ti
46.........	19	1.03	8	25	0.10	6	0.95	Ti
45.........	19	0.97	9	26	0.15	8	0.95	Sc
44.........	20	0.92	9	26	0.20	8	0.96	Ca
43.........	20	0.97	8	26	0.15	8	0.96	Ca
42.........	20	1.02	7	26	0.10	8	0.96	Ca
41.........	20	0.92	6	26	0.20	8	0.96	Ca
40.........	20	0.84	6	26	0.28	10	0.96	Ca
39.........	20	0.73	7	25	0.38	12	0.98	K
38.........	18	0.86	8	22	0.24	8	0.98	A
37.........	20	0.81	7	24	0.28	7	1.00	Cl
36.........	22	0.82	12	22	0.25	12	1.00	S
35.........	20	0.87	7	26	0.22	10	1.00	Cl
34.........	22	0.87	12	22	0.20	12	1.00	S
33.........	22	0.82	12	22	0.25	12	1.00	S
32.........	22	0.97	12	30	0.10	12	1.00	S
31.........	21	0.85	8	29	0.20	12	1.02	P
30.........	20	0.83	7	26	0.20	8	1.04	Si
29.........	20	0.83	7	26	0.20	8	1.04	Si
28.........	21	1.01	8	30	0.02	8	1.04	Si
27.........	21	0.80	8	29	0.20	12	1.05	Al
26.........	18	0.77	8	26	0.20	8	1.08	Mg
25.........	23	0.77	9	28	0.20	7	1.08	Mg
24.........	19	0.94	11	29	0.03	6	1.08	Mg
23.........	22	0.83	12	25	0.12	10	1.09	Na
22.........	22	0.81	12	21	0.11	4	1.09	Ne
21.........	22	0.84	12	25	0.08	6	1.09	Ne
20.........	22	0.87	12	26	0.05	8	1.09	Ne
19.........	23	0.76	14	29	0.14	14	1.10	F
18.........	24	0.67	9	29	0.20	10	1.10	O
17.........	24	0.77	9	29	0.20	10	1.10	O
16.........	24	0.83	9	30	0.04	10	1.10	O
15.........	23	0.73	10	23	0.10	10	1.07	N
14.........	23	0.46	10	23	0.37	10	1.07	N
13.........	23	0.71	8	27	0.05	8	1.06	C
12.........	23	0.76	6	...*	...	...	1.06	C
11.........	26	0.85	11	26	0.15	11	1.03	B
10.........	25	0.54	11	25	0.15	11	1.03	B
9.........	26	0.67	20	...*	...	...	1.00	Be
4.........	27	0.47	12	45	0.11	40	1.11	He
3.........	13	0.33	18	15	0.33	13	1.11	He
2.........	5	0.97	−3, +15	...	...	...	...	H

* Two nucleon emission negligible.

The quantity $\epsilon_{0,1}'$ equals the mean energy for the reaction $\sigma^{(1)}(\epsilon')$ chosen by inspection of a graph of the cross section as a function of ϵ'.

$$\Delta_1 \sigma_m = \int_0^{30} \sigma^{(1)}(\epsilon') d\epsilon' , \tag{8}$$

where the effective energy bandwidth Δ_1 and the mean cross section σ_m were chosen so as to closely as possible match the actual dependence of $\sigma^{(1)}(\epsilon')$ on energy.

The corresponding quantities for the two nucleon reactions were chosen in a similar way. As has been indicated previously, there are ample experimental data available for photon energies below 30 MeV to use in determining these parameters. For these excitation energies, the principal uncertainties in the final results are probably those associated with the very crude parameterization used to describe the one and two nucleon emission cross sections as a function of energy.

TABLE 2

BRANCHING RATIOS FOR i-NUCLEON EMISSION IN THE 30–150 MeV ENERGY RANGE

Nucleus	i	f_i	Main Channel
^{4}He.........	1	0.8	^{4}He (γ, n) ^{3}He, ^{4}He (γ, p) ^{3}H
	2	0.2	^{4}He (γ, np) ^{2}H
^{9}Be..........	1	1	^{9}Be (γ, n) 2^{4}He
^{10}B–^{22}Ne.....	1	0.1	
	2	0.3	
	3	0.1	
	4	0.1	
	5	0.2	
	6	0.2	
^{23}Na–^{56}Fe....	1	0.10	
	2	0.35	
	3	0.10	
	4	0.05	
	5	0.15	
	6	0.045	
	7	0.04	
	8	0.035	
	9	0.03	
	10	0.025	
	11	0.02	
	12	0.018	
	13	0.015	
	14	0.012	
	15	0.01	

The data for the region from 30 to 150 MeV are parameterized by two quantities, the total strength of the interaction given by ζ in Table 1, and a branching ratio given in Table 2. The total strength is given by

$$\zeta = \frac{1}{\sum_d} \int_{30}^{150} \sigma_t(\epsilon')d\epsilon' , \tag{9}$$

where $\sigma_t(\epsilon')$ is the total photonuclear absorption cross section. The strength between 30 and 150 MeV was actually obtained by taking the difference between the estimated total strength to 150 MeV and a value for the measured strength in the region 0 to 30 MeV. The estimated total strength to 150 MeV as a function of Z was based to a large extent on an interpolation and extrapolation of the total cross section measurements made at Mainz (J. Ahrens *et al.*, private communication, to be published in *Nuclear Physics*). These values are estimated to have an overall uncertainty of ± 15 percent. The branching ratio data given in Table 2 for the nuclei heavier than Na are based on spallation product yields induced by bremsstrahlung with peak energies ranging from 150 to 240 MeV, while the data for the lighter nuclei are based on the analysis of 170 MeV bremsstrahlung yields obtained from cloud chamber measurements. These data should not be taken to represent anything more than a first approximation of the yields that might be expected from a $1/\epsilon'$ photon energy spectrum.

For the lighter elements it is found that only about half of a "dipole sum" as given by equation (6) is in the giant resonance, and even for ^{39}K only about 3/4 of the value given in equation (6) is in the giant resonance. In the particular cases of elements with $A \leq 4$, the giant resonance does not play a role in the photodisintegration process (see later discussion). One may also note that in terms of total integrated cross sections

$$\int_0^{30\,\mathrm{MeV}} \sigma_t(\epsilon')d\epsilon' \approx \int_{30}^{150\,\mathrm{MeV}} \sigma_t(\epsilon')d\epsilon' , \tag{10}$$

indicating that nonresonant and higher order multipole processes make significant contributions to the total cross section for energies below 150 MeV.

III. INTERGALACTIC BACKGROUND RADIATION FIELDS

The background radiation of importance in determining the photonuclear reaction rate in intergalactic space consists of the 2.7 K microwave radiation and the radiation fields of higher energy, *viz*., the infrared and the optical background radiation. The long wavelength radio background from extragalactic sources (Clark, Brown, and Alexander 1970) is of too low an energy and intensity to be of importance in the context of this paper.

a) Microwave Radiation

The 2.7 K radiation appears, for all practical purposes here, to be an ideal blackbody in the energy range 2×10^{-6} eV $< \epsilon < 2 \times 10^{-3}$ eV (Peebles 1971; Thaddeus 1972; Hegyi, Traub, and Carleton 1974; Robson *et al.* 1974, Woody *et al.* 1975). We assume it to be such in our calculations. Figure 3 shows the assumed blackbody spectrum along with some sample data points (e.g., the solid lines show the data of Robson *et al.* and Woody *et al.*).

b) Optical Radiation

In considering the optical and infrared radiation in intergalactic space, one must keep in mind that even for measurements made outside the atmosphere, the measured background contains components from such nonextragalactic sources as zodiacal light, emission from interplanetary and interstellar dust, and radiation from nearby stars at high galactic latitutdes as well as halo stars. Therefore, because only upper limits are available from direct measurements, the intergalactic infrared and optical radiation must be estimated using theoretical arguments.

Measurements of the fluctuations of the observed optical background on a small angular scale give upper limits on the contribution to the extragalactic flux from discrete sources such as galaxies (Partridge 1974; Shectman 1974). The implied flux gives a value for the energy density of the optical radiation of $\sim 3 \times 10^{-3}$ eV cm^{-3} in the energy range 0.8 eV $< \epsilon <$ 10 eV. This value precludes strong evolution of the luminosity function for galaxies (i.e., galaxies much brighter in the past) as has been discussed by Partridge and Peebles (1967*a*, *b*). Of course, a diffuse field of truly extragalactic origin (e.g., bremsstrahlung from a hot intergalactic gas) would not be detectable using fluctuation measurements, but we can assume that such radiation is relatively small (Field 1972).

We therefore assume an intergalactic dilute starlight field with a temperature of 5000 K and a dilution factor of 1.2×10^{-15} in our calculations. The effect of such a field is small, as previously noted in the case of a somewhat larger optical radiation field by Stecker (1969).

c) Infrared Radiation (2×10^{-3} eV to 0.8 eV)

Only experimental upper limits exist in the infrared energy range for the extragalactic background radiation (Pipher *et al.* 1971; Soifer, Houck, and Harwit 1971; Houck *et al.* 1972; Muehlner and Weiss 1972; Williamson *et al.* 1973; McNutt and Feldman 1970; Hoffmann, Frederick, and Emery 1973). Thus we must rely on theoretical estimates of this radiation. Here, as in the case of the optical background radiation, we shall assume that the infrared background originates mainly in extragalactic objects. In the last four years it has been found that many of the active extragalactic objects such as quasars, N galaxies, the nuclei of Seyfert galaxies, and some radio galaxies as well, emit most of their energy in the far-infrared in the 30 to 100 μ range. Neugebauer, Becklin, and Hyland (1971), Rieke and Low (1972), and Kleinman and Wright (1974) give fluxes at 10 μ for 64 of these sources. For two sources, M82 and NGC 253, a continuous spectrum has been measured. If we use these data, combined with the data of Schmidt (1971) on the luminosity function of extragalactic objects, it is possible to evaluate the contribution of these extragalactic objects to the infrared background. The data indicate that a typical extragalactic infrared source has a maximum in its spectrum between 30 μ and 100 μ and that the average spectral index of its energy spectrum on the high-frequency side of the maximum is $\alpha \approx 1.5$.

The effect of sources at high redshifts z can be estimated as follows: If one considers a class of objects with a density evolution with redshift given by $n = n_0(1 + z)^m$ out to a maximum redshift z_M($m = 3$ being the case with no evolution and only geometrical expansion included) and we consider the part of their spectrum which has a power-law form so that their intensity is given by

$$I(\nu) = I_0\nu^{-\alpha} \quad \text{for} \quad \nu_m \leq \nu \leq \nu_M\,, \tag{11}$$

their integrated contribution to the infrared background is then of the form

$$F(\nu) = n_0 I_0 \nu^{-\alpha}(cH_0^{-1}/4\pi)\int_0^{z_M} dz(1 + z)^{m-(\alpha+5)}(1 + \Omega z)^{-1/2}\,, \tag{12}$$

where H_0 is the Hubble constant and Ω is the fraction of the critical density.

The solution to equation (12) will give power-law spectra in the frequency ranges $\nu_m(1 + z_M)^{-1} \leq \nu \leq \nu_m$ and $\nu_m \leq \nu \leq \nu_M$ with a spectral index depending on the values of α and m.

If most quasars have a high-infrared output compared with their output at other wavelengths, it then seems to be a likely possibility that there is a strong redshift evolution of their infrared luminosity as is found to be the case at optical wavelengths ($m = 6$). Considering the limited amount of observational data on Seyfert galaxies, both strong evolution ($m = 6$) and no evolution ($m = 3$) have been considered here in estimating their contribution to the infrared background. The fluxes from quasars and Seyfert galaxies, as well as the flux from normal galaxies with $m = 3$, have been computed and the results of these calculations are shown in Figure 3.

Two power laws have been drawn on Figure 3 which can be considered as giving reasonable lower and upper limits on the intergalactic infrared flux. At very long wavelengths ($\sim 500\,\mu$) the major contribution to the infrared

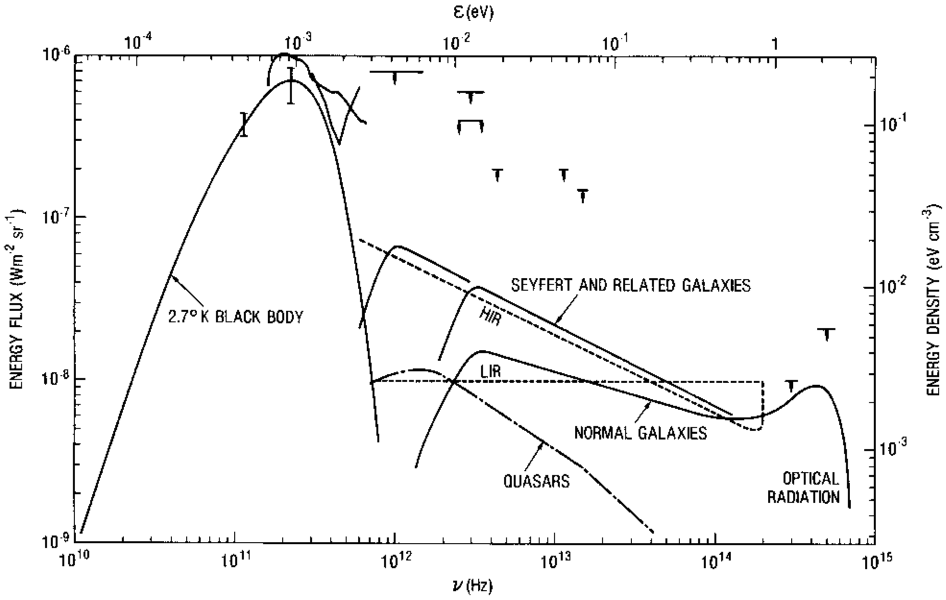

FIG. 3.—Computed background radiation fields from quasars, Seyfert and related galaxies, and normal galaxies as discussed in the text. Also shown are the 2.7 K microwave and optical radiation fields as well as some measured values and upper limits. The dotted lines labeled HIR and LIR were taken as alternative models for the intergalactic infrared background fields used in the calculations. Quantities given are equivalent to spectral densities times frequency (Hz per Hz).

background is probably due to the diffuse component associated with the distortion of the 2.7 K blackbody spectrum due to effects associated with the early thermal history of the Universe (Kompaneets 1957; Zel'dovich, Illariorov, and Sunyaev 1972; Chan and Jones 1975).

The power-law spectra shown in Figure 3, which were employed in this paper, were taken to extend from the optical graybody radiation field to the microwave blackbody radiation field. They will hereafter be designated as HIR (high infrared case) and LIR (low infrared case). They are given in terms of photon density spectra by the numerical expressions

$$\mathrm{HIR}: n(\epsilon) = 1.1 \times 10^{-3}\, \epsilon^{-2.5} \quad (\mathrm{cm}^{-3}\, \mathrm{eV}^{-1})$$

and

$$\mathrm{LIR}: n(\epsilon) = 2.6 \times 10^{-3}\, \epsilon^{-2} \quad (\mathrm{cm}^{-3}\, \mathrm{eV}^{-1}) \tag{13}$$

with the photon energies given in eV and the spectra extending over the energy range between 2×10^{-3} eV and 0.8 eV.

IV. CALCULATION OF THE INTERGALACTIC NUCLEON AND ENERGY LOSS RATES

The photodisintegration rate for a nucleus of mass A with the subsequent release of i nucleons is given by the expression

$$R_{A,i} = \tfrac{1}{2}\gamma_A^{-2} \int_0^\infty d\epsilon\, \epsilon^{-2} n(\epsilon) \int_0^{2\gamma_A \epsilon} d\epsilon' \epsilon' \sigma_{A,i}(\epsilon') \tag{14}$$

(Stecker 1969), where $n(\epsilon)$ is the photon density of the ambient radiation with energy ϵ in the observer's system (see previous section), ϵ' is the energy of the photon in the rest system of the cosmic ray nucleus, and γ_A is the Lorentz factor of the nucleus.

Because, as was discussed in § II, there can exist large and significant deviations from the pure Lorentzian shape in the energy range where the maximum cross section occurs, a Gaussian approximation for the cross section for one- and two-nucleon disintegrations in this energy range was found to be useful both as an adequate fit to the cross section data and as an expedient in performing the numerical calculations. This choice, in conjunction with a threshold energy of 2 MeV in the rest system of the nucleus[1] and a constant cross section above 30 MeV, was numerically found to give rates which were very similar to those given by a Lorentzian over the resonance region where integrated over the photon density function used in equation (14) as discussed in the previous section. The

[1] The physical cross sections have higher thresholds, but this makes little difference in the numerical calculations, since a Gaussian falls off much faster than a Lorentzian.

error introduced by this approximation was found to be relatively small compared with the other uncertainties involved in this calculation. Relatively more important was the consideration of multinucleon emission channels which, when weighted by the number of nucleons emitted, can be seen to have an important effect on the total nucleon and energy loss rates. This can be seen from an examination of the branching ratios for multinucleon emission given in Table 2.

The cross sections used for evaluating equation (14) were of the form

$$\sigma_{A,i} = W^{-1}\xi_{A,i}\sum_d \Delta_i^{-1}\theta_+(2)\theta_-(30)\exp\left[-2\left(\frac{\epsilon' - \epsilon_{0,i}'}{\Delta_i}\right)^2\right] + \frac{Sf_i\sum_d\theta_+(30)}{120} \tag{15}$$

for $i = 1, 2$, and

$$\sigma_{A,i} = \frac{Sf_i\sum_d\theta_+(30)}{120} \quad \text{for } i > 2\,, \tag{16}$$

where all the energies are in MeV and the normalization factor

$$W = \left(\frac{\pi}{8}\right)^{1/2}\left[\mathrm{Erf}\left(\frac{30 - \epsilon_{0,i}'}{2^{-1/2}\Delta}\right) + \mathrm{Erf}\left(\frac{\epsilon_{0,i}' - 2}{2^{-1/2}\Delta}\right)\right] \tag{17}$$

with

$$\mathrm{Erf}(x) = 2\pi^{-1/2}\int_0^x \exp(-t^2)dt \tag{18}$$

and

$$\begin{aligned} \theta_+(x) &= 1 \quad (\epsilon' \geq x) \\ &= 0 \quad (\epsilon' < x)\,, \\ \theta_-(x) &= 0 \quad (\epsilon' > x) \\ &= 1 \quad (\epsilon' \leq x)\,. \end{aligned} \tag{19}$$

By substituting equations (15) through (19) in equation (14), the photodisintegration rates can be expressed as sums of integrals of four basic forms. The first is

$$I_1 = \frac{C_1}{2\gamma_A^2}\left[\int_{2/2\gamma}^{30/2\gamma} d\epsilon(e^{-\epsilon/kT} - 1)^{-1}J(\epsilon) + \int_{30/2\gamma}^{\infty} d\epsilon(e^{-\epsilon/kT} - 1)^{-1}J'(\epsilon)\right] \tag{20}$$

for integrations of the Gaussian part of the cross section over a thermal photon field where

$$C_1 = (\pi^2\hbar^3c^3)^{-1}DW^{-1}\xi_{A,i}\textstyle\sum_d\Delta^{-1}\,, \tag{21}$$

D being a dilution factor for the case of starlight optical radiation (graybody) which is equal to unity for pure blackbody radiation. The functions $J(\epsilon)$ and $J'(\epsilon)$ are given by the expressions

$$\begin{aligned} J(\epsilon) = \int_{2\mathrm{MeV}}^{2\gamma\epsilon} xe^{-2\left(\frac{x - \epsilon_{0,i}'}{\Delta}\right)^2}dx &= \left(\frac{\pi}{8}\right)^{1/2}\epsilon_{0,i}'\Delta\left[\mathrm{sign}\,(2\gamma\epsilon - \epsilon_{0,i}')\,\mathrm{Erf}\left(\frac{2\gamma\epsilon - \epsilon_{0,i}'}{2^{-1/2}\Delta}\right) + \mathrm{Erf}\left(\frac{\epsilon_{0,i}' - 2}{2^{-1/2}\Delta}\right)\right] \\ &+ \left(\frac{\Delta}{2}\right)^2\left\{\exp\left[-2\left(\frac{\epsilon_{0,i}' - 2}{\Delta}\right)^2\right] - \exp\left[-2\left(\frac{2\gamma\epsilon - \epsilon_{0,i}'}{\Delta}\right)^2\right]\right\}, \end{aligned} \tag{22}$$

$$\begin{aligned} J'(\epsilon) = \left(\frac{\pi}{2}\right)^{1/2}\epsilon_{0,i}'\Delta\left[\mathrm{sign}\,(30 - \epsilon_{0,i}')\,\mathrm{Erf}\left(\frac{30 - \epsilon_{0,i}'}{2^{-1/2}\Delta}\right) + \mathrm{Erf}\left(\frac{\epsilon_{0,i}' - 2}{2^{-1/2}\Delta}\right)\right] \\ + \left(\frac{\Delta}{2}\right)^2\left\{\exp\left[-2\left(\frac{\epsilon_{0,i}' - 2}{\Delta}\right)^2\right] - \exp\left[-2\left(\frac{30 - \epsilon_{0,i}'}{\Delta}\right)^2\right]\right\}. \end{aligned} \tag{23}$$

The second basic integral is of the form

$$I_2 = C_2/(2\gamma^2)\int_{\Delta}^{\epsilon_M} d\epsilon\,\epsilon^{-(\alpha+2)}J(\epsilon)\,, \tag{24}$$

where $\Lambda = \text{Max}\ \{\epsilon_m, 2\ \text{MeV}/2\gamma\}$, for integrations over the Gaussian part of the cross section and a power-law photon field existing over the energy range $\epsilon_m \leq \epsilon \leq \epsilon_M$ with the form

$$n(\epsilon) = K\epsilon^{-\alpha}\,. \tag{25}$$

The constant C_2 in equation (24) has the value

$$C_2 = KW^{-1}\xi_{A,i} \sum_{d} \Delta^{-1}\,. \tag{26}$$

The other two integrals are those over the high-energy nonresonant part of the cross section above 30 MeV. With the cross section $\sigma_{A,i}$ = constant over this energy range as given by equation (16), the relevant integrals take the form

$$I_3 = (\pi^2\hbar^3c^3)^{-1}D\sigma_{A,i}\left[\int_{30/2\gamma}^{\infty} \frac{\epsilon^2 d\epsilon}{e^{\epsilon/kT} - 1} - \left(\frac{30}{2\gamma}\right)^2 \int_{30/2\gamma}^{\infty} \frac{d\epsilon}{e^{\epsilon/kT} - 1}\right] \tag{27}$$

for a thermal photon spectrum $n(\epsilon)$ and

$$I_4 = K\sigma_{A,i}\left[\int_{\Upsilon}^{\epsilon_M} d\epsilon\, \epsilon^{-\alpha} - \left(\frac{30}{2\gamma}\right)^2 \int_{\Upsilon}^{\epsilon_M} d\epsilon\, \epsilon^{-(\alpha+2)}\right] \tag{28}$$

where $\psi = \text{Max}\{\epsilon_m, 30/2\gamma\}$, in the case of a power-law photon spectrum.

Equations (27) and (28) assume a constant cross section for all ϵ' above 30 MeV. In reality, photopion production becomes important above 150 MeV and changes the shape of the cross section. However, because of the steeply falling nature of the photon spectrum at high energies, these effects are not important for nuclei with Lorentz factors below 10^{11} (energy per nucleon below 10^{11} GeV).

Equation (14) was evaluated numerically using the above formulae in conjunction with the data given in Tables 1 and 2. Photodisintegration rates for nuclei with atomic mass numbers up to 56 were thereby evaluated. (For the three nuclei ^{3}He, ^{4}He, and ^{9}Be with nonresonant channels having large values of $\Delta[\Delta \gg 10\ \text{MeV}]$, the 30 MeV cutoff formalism was not employed.)

Figures 4 through 6 show samples of the results obtained giving $R_{A,i}^{-1}$ as a function of γ. It is interesting to note how the width of the low-energy part of the cross section Δ affects the rate calculations for $\gamma \approx 3 \times 10^9$. Another important effect is the difference in the energy dependence between the reaction channels dominated by the giant resonance ($i = 1, 2$) and those channels which only contribute to the high-energy part of the cross section. By combining the rates from all the reaction channels for a given nucleus, the effective nucleon loss rate for the nucleus can be calculated from the relation

$$R_{\text{eff},A} = (dA/dt) = \sum_{i} iR_{A,i}\,. \tag{29}$$

The quantity $R_{\text{eff}}^{-1}(\gamma)$ is shown in Figure 7 for ^{56}Fe along with the single emission time scale $R_{56,1}^{-1}$ in order to demonstrate the importance of multinucleon emission processes in determining the effective nucleon loss rate.

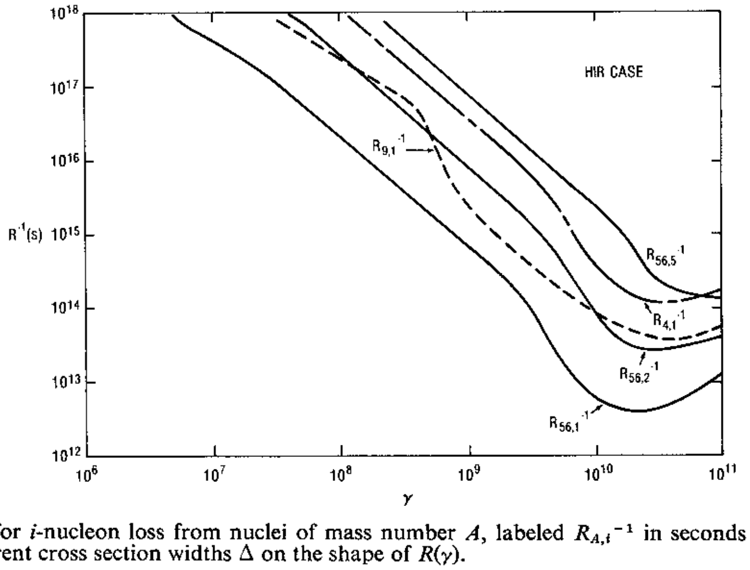

FIG. 4.—Inverse rates for i-nucleon loss from nuclei of mass number A, labeled $R_{A,i}^{-1}$ in seconds for an appropriate sample showing the effect of different cross section widths Δ on the shape of $R(\gamma)$.

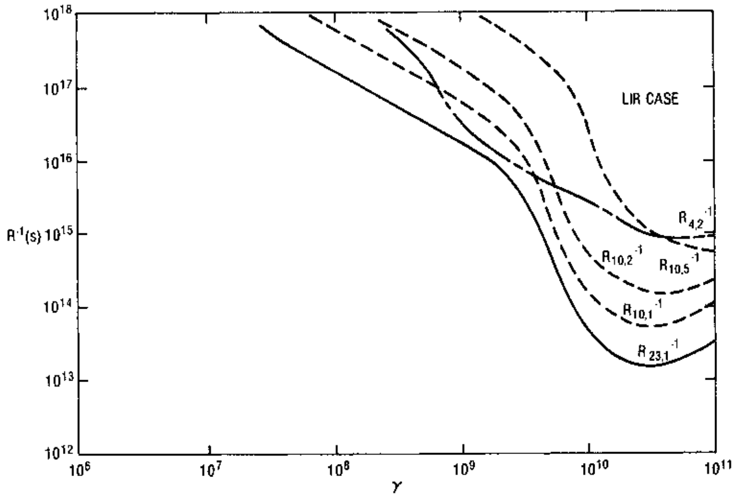

FIG. 5.—More sample inverse rates (see caption for Fig. 4)

The different energy loss rates for nuclei can now be compared. Figure 8 shows the characteristic energy loss time scale $\tau_E = (dE/dt)^{-1}E$ for ^{56}Fe from the effect of redshift losses, photodisintegration, and pair production losses. The photodisintegration time scale is shown for both the LIR and HIR cases. It can be seen that for ^{56}Fe, the energy loss rates from pair production and photodisintegration are comparable in the energy range near 10^{20} eV.

For photodisintegration, the average fractional energy loss rate

$$E^{-1}(dE/dt) = A^{-1}(dA/dt) \tag{30}$$

because the nucleon emission is isotropic in the rest system of the nucleus. The Lorentz factor, which is equivalent to energy per nucleon, is conserved for photodisintegration as opposed to the pair production and photopion production processes which involve the creation of new particles which carry off energy.

The energy loss time for pair production $\tau_{E,pp} \propto AZ^{-2}$ is implied by equation (4) which increases $\sim A^{-1}$. The energy loss time from photodisintegration implied by equation (30) is almost independent of A. Thus the relative importance of pair production as an energy loss process vis-à-vis photodisintegration decreases with decreasing Z when we consider nuclei lighter than iron.

V. MONTE CARLO CALCULATIONS OF THE PHOTODISINTEGRATION HISTORIES OF NUCLEI

As can be seen from the results of the previous section, the photodisintegration rates for all nuclei have typically steep γ dependences. Pair production can also be quite sensitive to γ. Photodisintegration conserves γ, but pair

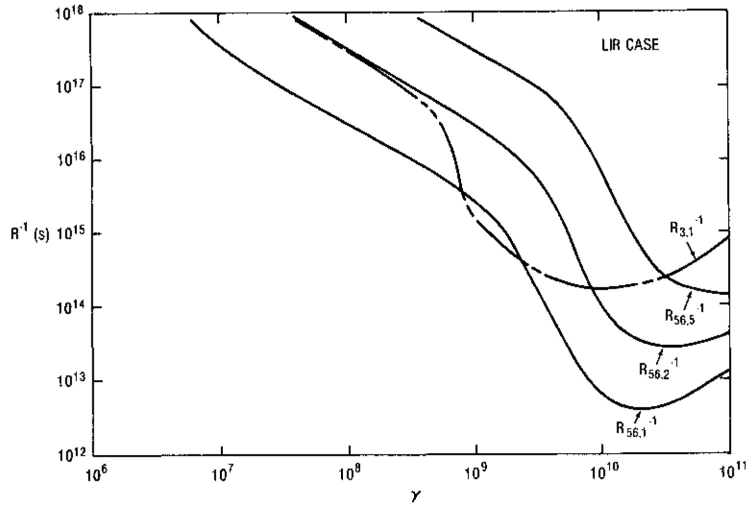

FIG. 6.—More sample inverse rates (see caption for Fig. 4)

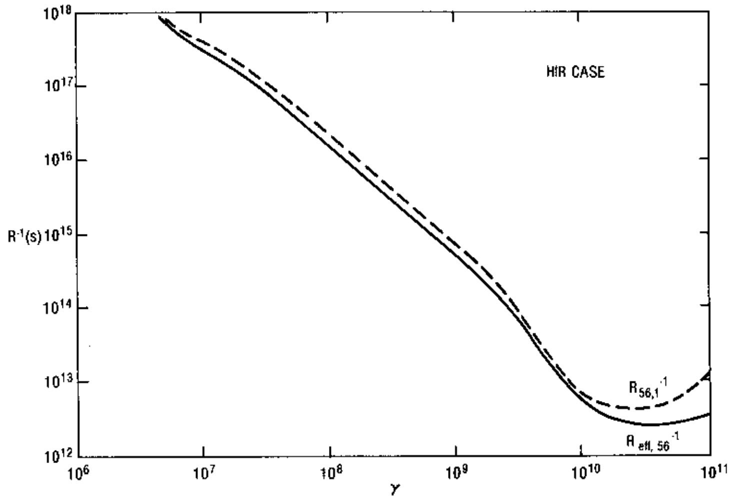

FIG. 7.—The effective inverse nucleon loss rate for ^{56}Fe shown along with the single emission time scale to demonstrate the importance of multinucleon emission processes.

production losses continually and cumulatively act to decrease the value of γ thereby directly affecting the photodisintegration rate. Thus, after a given period of time, nuclei with the same initial value of γ acquire differing new values of γ depending on their individual disintegration histories $A(t)$ due to the interplay of the differing energy loss processes. The only way to take correct account of the effect of changes in γ and A with time is to keep track of each individual nucleus as it cascades down in A. This is especially important for the low infrared (LIR) case.

These considerations lead us to use a Monte Carlo technique to compute the behavior of nuclei starting at various initial values of γ (designated by γ_0). At each step, each nucleus followed in the calculation is characterized by the two quantities A_k and γ_k (k being the step number). For a given time step, the probability of each reaction A_k going to $A_k - i$ can be calculated using the rates computed previously as functions of γ. The step size Δt is chosen so that the sum of the probabilities for all possible i is smaller than 1, the difference from unity being the

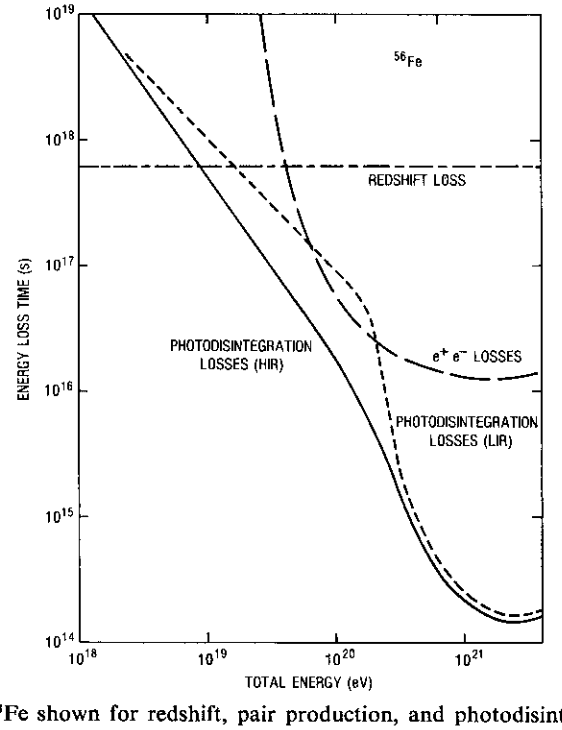

FIG. 8.—Energy loss time for ^{56}Fe shown for redshift, pair production, and photodisintegration losses in the HIR and LIR cases.

probability for no interactions in a time Δt. Since photodisintegration conserves γ, the new value of γ is then computed for each nucleus using the pair production rate.

Using the Monte Carlo technique, for each step we randomly determine the reaction channel for each nucleus in the system by assigning a random number to the nucleus and associating the occurrence of a particular channel with a set of such numbers such that the size of the set is proportional to the branching ratio for that channel. The Principle of Large Numbers then states that, given enough nuclei in the system considered, the frequency of random occurrences followed in the calculation will reflect the true probability distribution of the reactions as determined by their branching ratios.

The complete photodisintegration of iron takes, on the average, about 20 events if one includes multinucleon channels, which indicates that choosing a computation run involving a few hundred time steps corresponds to a small interaction probability for each step. The total number of particles in the system must also be such that the number of particles having a value A near $\langle A\rangle$ at a given time t is large enough so that a fair representation of the branching ratios of different reaction channels can be obtained after they all undergo one interaction.

For each initial value γ_0 used in a computation run, 500 particles were followed in the photodisintegration cascade. The partial results of two such runs are shown in Figure 9 (Plate 12) which shows the computed histories of two beams of ^{56}Fe nuclei starting out at different initial energies. For comparison, we also indicate in the figure the lifetime for ^{56} Fe against one nucleon loss for each initial energy. These runs were made using the HIR case, and it is quite obvious that, even in this case, the lifetime for complete photodisintegration of iron is $\sim$200 times higher than for the single nucleon loss process. Figure 10 shows the computed values of $\langle\gamma(t)\rangle$ for various values of γ_0 for ^{56}Fe. Also shown for comparison is the function $\gamma(t)$ for energy loss of protons from pair production for one typical value of γ_0.

In a few test cases, the same cascade was run several times with a different set of random numbers and different values of Δt. Typical differences in $\langle A\rangle$ introduced by such changes were of the order of $\leqslant 1$ percent. This proved that the number of particles and time steps used in the computation yielded results with adequate precision.

Using the computed values of the functions $\langle A(t)\rangle$ and $\gamma(t)$ obtained for different initial energies, the effect of photodisintegration on a power-law initial energy distribution can be calculated. This procedure is preferable to the introduction of a power-law distribution in energy of the nuclei used in a Monte Carlo run in which case poorer results are obtained because in that case inefficiencies would result from there being either too many or too few particles in some energy ranges due to the steepness of the initial spectrum.

For comparison with the results of the Monte Carlo calculation, the quantity dA/dt for ^{56}Fe shown in Figure 7 can be used together with the approximation that the photodisintegration cross section scales like $NZ/A \approx A/4$. Thus, for the HIR case for which photodisintegration is significantly more important than pair production[2]

$$\left.\frac{dA}{dt}\right|_A \approx \left.\frac{dA}{dt}\right|_{\mathrm{Fe}}\left(\frac{A}{56}\right) \tag{31}$$

which implies that $A(t)$ is an exponential function of time with an e-folding time of $56(dA/dt)_{\mathrm{Fe}}{}^{-1}$. Figure 11 shows the function $\langle A(t)\rangle$ obtained from the Monte Carlo calculations for various γ_0 for both the HIR and LIR cases.

[2] The actual dependence of the photodisintegration cross section on A is somewhat higher as can be seen from the values of ξ given in Table 1.

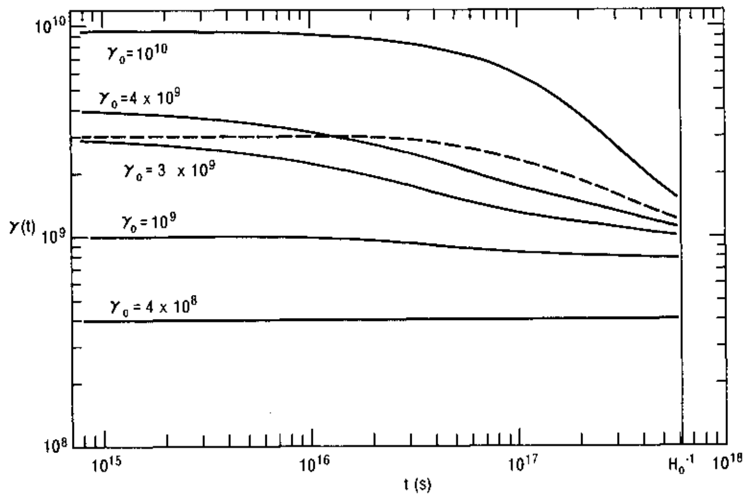

FIG. 10.—The computed value of $\gamma(t)$ for ^{56}Fe with given initial values γ_0 shown by the solid lines. The dashed line shows the function $\gamma(t)$ for protons with $\gamma_0 = 3 \times 10^9$ for comparison.

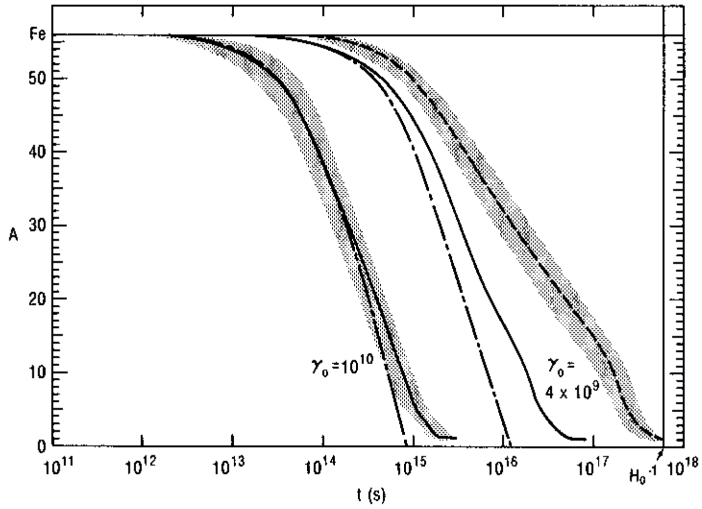

FIG. 11.—Sample values of $\langle A(t)\rangle$ for two values of γ_0. The HIR case is shown by the solid lines, the LIR case is shown by the dashed line, and the scaling approximation (see text) is shown by the dot-dash line.

We also show for comparison the value of $A(t)$ obtained under the approximation given by equation (31). In the HIR case, A is not decreasing as fast as the simple scaling approximation (31) would imply because of the diminishing relative importance of multinucleon channels for lighter nuclei. For the LIR case it is apparent that more than just a change in the photodisintegration rate is occurring because of the definite change in the character of the function $A(t)$ for $t \gtrsim 5 \times 10^{15}$ s. This change is due to the effect of pair production on γ which can be seen to be qualitatively more than a small correction and illustrates the rationale for using the Monte Carlo method in order to obtain results which are truly valid. The shaded areas around the curves shown in Figure 11 show the one standard deviation spread in A around $\langle A\rangle$ determined from the Monte Carlo computations from more detailed information as illustrated in Figure 9. More $\langle A(t)\rangle$ curves are shown in Figure 12. By combining these $\langle A(t)\rangle$ results with those on $\gamma(t)$ for various values of γ_0, one can obtain the function $\langle A(\gamma_f)\rangle$ where γ_f is the final value of γ for nuclei starting out as Fe after some time t when they have disintegrated to nuclei of mass A. This function for various values of t is shown in Figure 13.

VI. ASTROPHYSICAL IMPLICATIONS OF THE RESULTS

The results of the Monte Carlo computations discussed in the previous section can be used to discuss the effect of photonuclear emission processes on ultrahigh energy nuclei in intergalactic space by evaluating their effect on an initial beam of ^{56}Fe nuclei with a power-law energy spectrum at injection. One may then ask how this energy

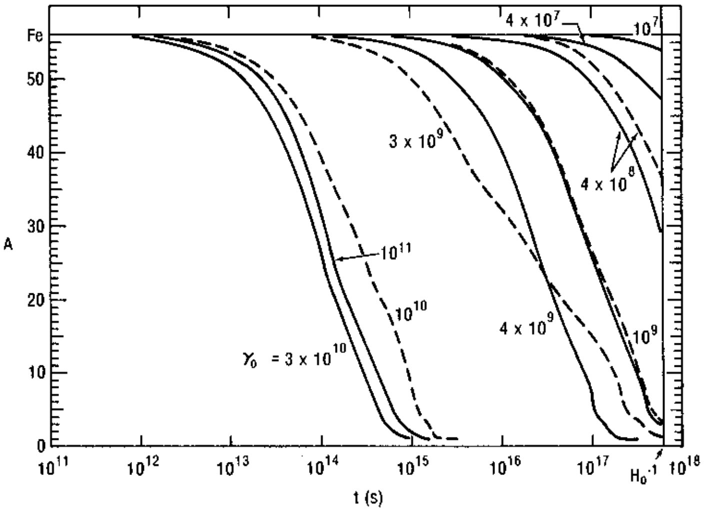

FIG. 12.—More sample values of $\langle A(t)\rangle$. *Solid lines*, HIR case; *dashed lines*, LIR case.

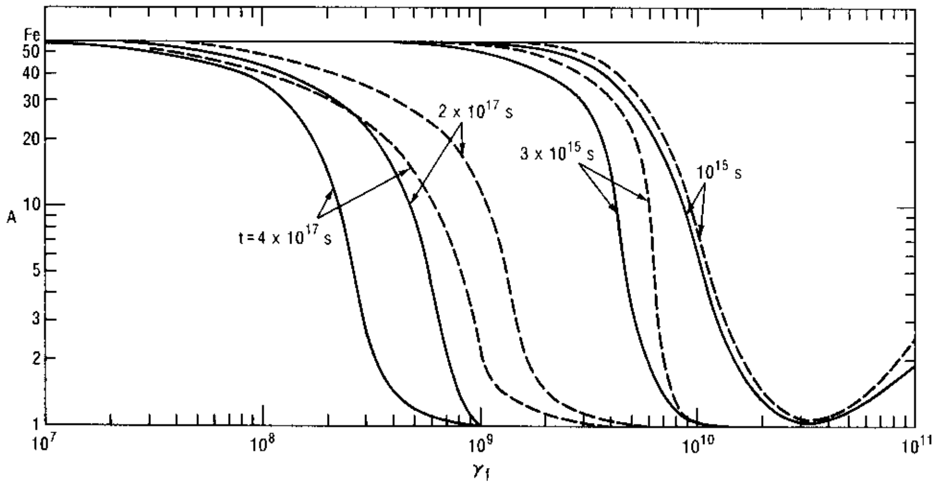

FIG. 13.—The function $A(\gamma_f)$ calculated for various time scales of astrophysical significance. *Solid lines*, HIR case; *dashed lines*, LIR case.

spectrum changes after a given period of time corresponding to the mean age of the nuclei under various assumptions as to their origin. The predicted characteristics of the ultrahigh energy cosmic rays under these various assumptions may then be compared with the data regarding the energy spectrum of ultrahigh energy cosmic rays given in terms of total energy per nucleus from air-shower observations.

We shall consider here two hypotheses of particular astrophysical significance, *viz.*, the universal origin hypothesis and the local supercluster origin hypothesis. For the universal origin hypotheses, we can consider that cosmic rays have been produced at a roughly uniform rate throughout a time t_H which is related to the Hubble constant H_0 and given by $\frac{2}{3}H_0^{-1}$ for an Einstein–de Sitter universe and H_0^{-1} for a low-density universe where H_0 is taken to be 50 km s^{-1} Mpc. The average age of the cosmic rays is then $t_H/2$.

For the supercluster origin hypothesis, we assume that most of the cosmic rays we observe at ultrahigh energy are produced within the local supercluster of galaxies which is centered on the populous Virgo cluster at a distance of $\sim$20 Mpc and of which our Galaxy is considered to be a member. Under this hypothesis, the average age of the ultrahigh energy cosmic rays will be $\sim 2 \times 10^{15}$ s.

Of course, an equilibrium spectrum of such cosmic rays produced from a uniform distribution of sources will contain a spread in values of A at a given value of γ. Nevertheless, the functions shown in Figures 11 and 12 giving $A(t)$ show that a dispersion of a factor of 2 in the age introduces a dispersion in A which is not larger than the dispersion introduced by the cascade process itself. To simplify the discussion we shall first consider the time behavior of a power-law energy spectrum of Fe nuclei injected in a burst at an initial time $t = 0$. If we start with such an initial spectrum $J(\gamma_0)$ and know that $\gamma_f(t)$ and $A(t)$, there are then two well-defined functions $\gamma_f(\gamma_0)$ and $A(\gamma_f)$. This is because the change in γ with time is determined by the pair production and redshift energy loss rates and the photodisintegration process changes A without changing γ. The spectrum in γ_f at time t is then obtained from the inverse function $\gamma_0(\gamma_f)$ numerically evaluating the relation

$$I(\gamma_f; t) = (d\gamma_0/d\gamma_f)J[\gamma_0(\gamma_f)] . \tag{32}$$

The final energy of the nuclei is, of course, $E = \gamma_f A(\gamma_f)m_p$. $E(\gamma)$ is a nonmonotonic function which reaches a maximum at a critical energy E_c, then decreases again to a minimum and starts increasing again with γ. This implies that nuclei having an energy $E = E_c + \delta E$ must have started out with an initial γ_0 much larger than those having an energy E_c because of the rapid change of A with γ from photodisintegration. Naturally, those nuclei having started out with a much higher value of γ_0 were produced with a much lower intensity. The physical result of this is then that there is a resultant discontinuity or effective cutoff in the predicted equilibrium spectrum at an energy E_c. In reality, the cutoff will not be infinitely sharp because of the dispersion in A associated with the cascade (see, e.g., Fig. 11) and the dispersion in age of the cosmic rays due to the spatial distribution of the sources. Nonetheless, there will be a sharp drop in the cosmic-ray intensity near the value of E_c associated with the mean age of the cosmic rays.

Starting with an injection spectrum $J(\gamma_0) \propto \gamma_0^{-3}$, the resultant spectrum $I(E; t)$ was calculated for various values of t associated with the universal origin and supercluster origin hypotheses. The function $E^3I(E; t)$ is plotted in Figure 14 for the HIR case and in Figure 15 for the HIR case, given in arbitrary units. By comparison, the observational data on the energy spectrum $E^3I(E)$ as given by Hillas (1974) do not show any attenuation effects and are consistent with a straight horizontal line $[I(E) \propto E^{-3}]$ up to the highest observed energy of $\sim 2 \times 10^{20}$ eV.

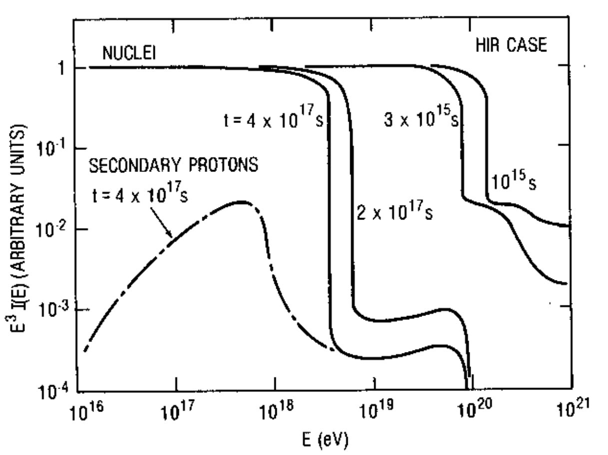

FIG. 14

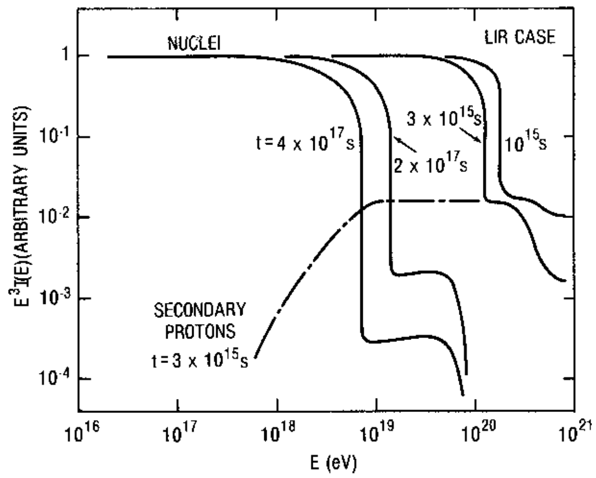

FIG. 15

FIG. 14.—Calculated shape of the ultrahigh energy cosmic ray spectrum after a time t from injection of a γ^{-3} primary ^{56}Fe spectrum given as $E^3I(E)$ in arbitrary units for the HIR case and astrophysically significant time scales with the effect of secondary protons included.

FIG. 15.—Calculated shape of the ultrahigh energy cosmic ray spectrum in the LIR case (see caption for Fig. 14).

The value of E_c given as a function of time is shown in Figure 16. From this figure, it can be seen that a typical dispersion in cosmic ray age of a factor of 2 will produce a change in E_c by less than a factor of 2 so that the predicted cutoff energy as a function of cosmic-ray age is quite well defined. Thus the low cutoff energy predicted for the universal cosmic-ray hypothesis on the assumption that the initial cosmic rays are intermediate mass nuclei is in clear contradiction with the observations. In the case of the supercluster hypothesis, however, the predicted cutoff energy is too close to the upper limit of the observations, especially considering the error involved in determining the energy of a shower-producing particle in the 10^{20} eV range, to imply any contradiction. Although the results shown in Figures 14 and 15 are given for an initial composition of ^{56}Fe, the values of E_c for nuclei of lower $\langle A \rangle$ will be even lower because $E \propto A$ for a given value of γ and the characteristic energy loss rate from photodisintegration is almost independent of A at a given value of γ.

The secondary nucleons produced in the photodisintegration reactions, which eventually become protons, are emitted isotropically in the rest frame of the parent nuclei and thus have, on the average, the same Lorentz factor as the parent. These secondaries lose energy through pair production and photomeson production interactions at a rate which is slower than that of the parent nuclei. Nevertheless, for a given value of γ_0 such that γ_f is a fairly good approximation for the average γ of the secondaries. The spectra of the secondaries obtained under this approximation are shown in Figures 14 and 15 assuming no cutoff in the injection spectrum. For energies above E_c, for which

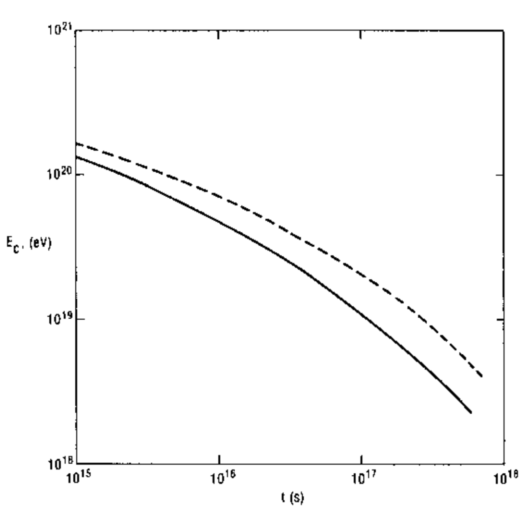

FIG. 16.—Value of the calculated cutoff energy E_c for ultrahigh energy cosmic rays starting out as Fe and evaluated after a time t. These values are given for the HIR case by the solid line and the LIR case by the dashed lines.

the secondaries are dominant, the value of γ_0 associated with their parent primaries is very large, and the associated value of A has been 1 for most of the time considered, making our approximation a good one. It can be seen that the existence of a secondary proton component does not affect our prediction of a sharp cutoff in the observed spectrum at E_c.

VII. CONCLUSIONS

The results of this paper indicate that because of the lack of attenuation effects in the observed spectrum up to 1 to 2×10^{20} eV, ultrahigh energy cosmic rays cannot be universal in origin *regardless of whether they are protons or nuclei.* (The cutoff energy for protons can be seen from Fig. 2 to occur at $\sim 5 \times 10^{19}$ eV due to photomeson production losses with a lower energy steepening predicted to occur at $\sim 2 \times 10^{18}$ eV due to pair production.) Both the supercluster and galactic origin hypotheses, however, are possible for protons (Stecker 1968) *and higher mass nuclei.*[3]

These conclusions are further supported by reports of a distinct anisotropy in the arrival directions of cosmic rays at ultrahigh energies (Krasilnikov *et al.* 1974, Linsley 1975 and private communication; Edge *et al.* 1975), again arguing against a universal origin for these cosmic rays, since a universal origin implies large-scale isotropy.[4]

When measurements of the mean mass of cosmic rays in the 10^{17} to 10^{19} eV energy range become available, the results given here for $A(\gamma_f)$ as shown in Figure 13 can be used to help determine their age and origin further. Should it be found in the future that the cosmic ray spectrum continues to values of total energy much in excess of 10^{20} eV, this would rule out their being of mixed or intermediate mass composition or of intermediate mass origin even under the supercluster origin hypothesis.

Note added in proof.—At the recent 14th International Cosmic Ray Conference, four papers were presented examining the problem of the distintegration of ultrahigh energy cosmic-ray nuclei. Two of these (V. S. Berezinskii, S. I. Grigor'eva and G. T. Zatsepin, *Proc. 14th Int. Cosmic Ray Conf.*, **2**, 711; A. M. Hillas, *ibid.*, p. 717) concluded that the universal origin hypothesis is not consistent with the present air-shower data. In the model discussed in the third paper (W. Tkaczyk, J. Wdowczyk, A. W. Strong, and A. W. Wolfendale, *ibid.*, p. 729), the *observed* cosmic rays at the highest energies have ages less than 3×10^{15} s, consistent with a supercluster origin hypothesis (Stecker 1968). The fourth paper (J. L. Puget and F. W. Stecker, *ibid.*, p. 734) was a preliminary version of the present work.

We wish to gratefully acknowledge Dr. E. G. Fuller for compiling the photonuclear cross section data from the files of the U.S. National Bureau of Standards and for communicating it to us in a form suitable for astrophysical calculations. We feel that without this data, a calculation of the type presented here could not have been properly performed.

[3] If we use new estimates of the infrared radiation field in the inner galaxy, as well as estimates of the galactic optical photon field, it can be shown that photodisintegration of nuclei traveling typical galactic distances is negligible. For a further discussion of the galactic origin hypothesis for ultrahigh energy cosmic rays, see Stecker (1971) and Syrovatskii (1971).

[4] Events reported coming from the direction of the north galactic pole may indeed originate near the heart of the Virgo (local) supercluster.

REFERENCES

Berezinskii, V. S., and Zatsepin, G. T. 1971, *Soviet J. Nucl. Phys.*, **13**, 453.
Blumenthal, G. R. 1970. *Phys. Rev.*, **D1**, 1596.
Chan, K. L., and Jones, B. J. T. 1975, *Ap. J.*, **195**, 1.
Clark, T. A., Brown, L. W., and Alexander, J. K. 1970, *Nature*, **228**, 847.
Danos, M., and Fuller, E. G. 1965, *Ann. Rev. Nucl.*, **15**, 29.
Edge, D. M., Reid, R. J. D., Watson, A. A., and Wilson, J. G. 1975, *Proc. 14th Int'l Cosmic Ray Conf.*, **2**, 604.
Field, G. 1972, *Ann. Rev. Astr. and Ap.* **10**, 227.
Gorbunov, A. N. 1968, *Phys. Letters*, **27B**, 436.
Greisen, K. 1966, *Phys. Rev. Letters*, **16**, 748.
Hayward, E. 1970, *NBS Monog. No. 118.*
Hegyi, D. J., Traub, W. A., and Carleton, N. P. 1974, *Ap. J.*, **190**, 543.
Hillas, A. M. 1974, *Phil. Trans. Roy. Soc. London A*, **277**, 413.
Hoffmann, W. F., Frederick, C. L., and Emery, R. J. 1971, *Ap. J.*, **170**, L89.
Houck, J. R., Soifer, B. T., Harwit, M., and Pipher, J. L. 1972. *Ap. J.*, **178**, L29.
Kleinman, D. E., and Wright, E. L. 1974, *Ap. J.*, **191**, L19.
Kompaneets, A. S. 1957. *Soviet Phys.—JETP*, **4**, 730.
Krasilnikov, D. D., Kuzmin, A. J., Linsley, J. Orlov, V. A., Reid, R. J. O., Watson, A. A., and Wilson, J. G. 1974, *J. Phys. A*, **7**, L176.
Levinger, J. S. 1951. *Phys. Rev.* **84**, 43.
Linsley, J. 1975, *Proc. 14th Int'l. Cosmic Ray Conf.*, **2**, 598.
McNutt, D. P., and Feldman, P. D. 1970, *Science*, **167**, 1277.
Muehlner, D., and Weiss, R. 1973. *Phys. Rev.*, **D7**, 326.
Neugebauer, G., Becklin, E., and Hyland, A. R. 1971, *Ann. Rev. Astr. and Ap.*, **9**, 67.
Partridge, R. B. 1974, *Ap. J.*, **192**, 241.
Partridge, R. B., and Peebles, P. J. E. 1967*a*, *Ap. J.*, **147**, 868.
———. 1967*b*, *ibid.*, **148**, 377.
Peebles, P. J. E. 1971, *Physical Cosmology* (Princeton: Princeton University Press).
Pipher, J. L., Houck, J. R., Jones, B. W., and Harwit, M. 1971, *Nature*, **231**, 375.
Rieke, G. H., and Low, F. J. 1972, *Ap. J.*, **176**, L95.
Robson, E. I., Vickers, D. G., Huizinga, J. S., Beckman, J. E., and Clegg, P. E. 1974, *Nature*, **251**, 591.
Schmidt, M. 1971, in *Nuclei of Galaxies*, ed. D. J. K. O'Connell (Amsterdam: North Holland), p. 395.
Shectman, S. A. 1974, *Ap. J.*, **188**, 233.
Soifer, B. T., Houck, J. R., and Harwit, M. 1971, *Ap. J.*, **168**, L73.
Stecker, F. W. 1968, *Phys. Rev. Letters*, **21**, 1016.
———. 1969, *Phys. Rev.*, **180**, 1264.

Stecker, F. W. 1971, *Nature Phys. Sci.*, **234**, 28.
Syrovatskii, S. I. 1971, *Comm. Ap. and Space Phys.*, **3**, 155.
Thaddeus, P. 1972. *Ann. Rev. Astr. and Ap.*, **10**, 305.
Williamson, K. D., Blair, A. G., Catlin, L. L., Hiebert, R. D., Loyd, E. G., and Romero, H. V., 1973, *Nature Phys. Sci.*, **241**, 79.
Woody, D. P., Mather, J. C., Nishioka, N. S., and Richards, P. L. 1975, *Phys. Rev. Letters*, **34**, 1036.
Zatsepin, G. T., and Kuz'min, V. A. 1968, *Soviet Phys.—JETP Letters*, **4**, 78.
Zel'dovich, Ya. B., Illarionov, A. F., and Sunyaev, R. A. 1972, *Eksperi Teoret. Fiz.*, **62**, 1217.

J. L. PUGET: Observatoire de Meudon, Section d'astrophysique, 92190, Meudon, France

F. W. STECKER and J. H. BREDEKAMP: Theoretical Studies Group, NASA Goddard Space Flight Center, Greenbelt, MD 20771

ABSTRACTS OF ASTROPHYSICAL JOURNAL SUPPLEMENT SERIES FOR THE 1976 MAY ISSUE

U CEPHEI: A MASS-TRANSFER EVENT. II. OBSERVATIONS

EDWARD C. OLSON
Department of Astronomy, University of Illinois

In late 1974, a major mass-transfer event occurred in the Algol-type eclipsing binary system U Cep. Strong photometric contamination during the nominally total primary eclipse was produced by the main mass-transferring stream, by a hot spot on the B-primary star, and by a disk around the primary (Olson 1976). A lower limit to the peak mass-transfer rate of 3×10^{-5} solar masses per year was deduced.

The above discussion was based on four-color *uvby* and β photoelectric observations, obtained with the 1 m reflector of the Prairie Observatory. The present paper summarizes the observational procedures and photometric reductions, and tabulates all observations.

REFERENCE

Olson, E. C. 1976, *Ap. J.*, **204**, 141.

NEW COLOR-MAGNITUDE DIAGRAMS FOR FOUR SOUTHERN GLOBULAR CLUSTERS

WILLIAM E. HARRIS, RENÉ RACINE, AND JAMES DE ROUX
David Dunlap Observatory

New photoelectric and photographic *BV* photometry is reported for the globular clusters NGC 6254 (M10), NGC 5286, NGC 5986, and NGC 6273 (M19).

M10 belongs to the M13–NGC 6752 class of clusters having extremely blue horizontal branches despite their appreciable metallicity ([Fe/H] ≈ -1.5). The relative number of UV–bright stars in M10 is the largest known. Significant discontinuities in the luminosity function of the cluster's giant branch are identified. At a distance of only 4.4 $\pm$ 0.3 kpc from the Sun, M10 is one of the nearest globular clusters.

Our exploratory study of the other three clusters leads to distances [assuming M_V(HB) $= +0.6$] as follows: NGC 5286, 8.7 $\pm$ 0.7 kpc; NGC 5986, 11 $\pm$ 1.3 kpc; NGC 6273, 10 $\pm$ 1.5 kpc. All three appear to be of moderately low metallicity with well-populated blue horizontal branches.

s-PROCESS STUDIES: BRANCHING AND THE TIME SCALE

RICHARD A. WARD, MICHAEL J. NEWMAN, AND DONALD D. CLAYTON
Department of Space Physics and Astronomy, Rice University

The theory of *s*-process heavy-element formation is reformulated to allow for competition between beta decay and neutron capture at various nuclei along the path. Solutions to the resulting branching network equations are presented (under the assumption of constant temperature and neutron flux) that do not require steady flow for the neutron current. Using the exponential exposure distribution $\rho(\tau) = G \exp(-\tau/\tau_0)$ and recently calculated temperature-dependent beta-decay rates, comparison of several key branches yields the following *average* conditions for the solar-system *s*-process environment: $T \approx 3.1 \times 10^8$ K, $n_n \approx 1.6 \times 10^7$ neutrons cm^{-3}. For $\tau_0 = 0.25\, n$ mb^{-1} we find that about 4.8 neutron captures per exposed iron seed are required over a time of the order of a few thousand years for synthesis of the bulk of the solar-system *s*-process material, with an average neutron capture time $\sim$10 years (for $\sigma \sim 500$ mb).

1976ApJ...205..638P

HIGH TIME-RESOLUTION OBSERVATIONS OF UV CETI STARS

THOMAS J. MOFFETT
Department of Astronomy, The University of Texas at Austin; and McDonald Observatory
AND
BERNARD W. BOPP
Ritter Observatory, The University of Toledo

Simultaneous, high time-resolution spectroscopic and photometric observations of eight flare events on four UV Ceti–type stars are presented. These observations firmly establish the existence of two phases during a flare: the spike phase, which is dominated by continuum emission, and the slow phase, which shows strong emission-line radiation with decreasing continuum radiation. The time sequence of spectral features during a flare is that the continuum reaches maximum strength first, followed 1 to 19 minutes later by maximum strength in the Balmer emission lines, and finally the peak of the Ca II K-line strength some 4 to 52 minutes after the continuum peak. The flare phenomenon is spectroscopically complex, with no apparent simple relation between the various flare parameters. The emission lines produce a time-varying contribution to the broad-band color indices of flare light.

IDENTIFICATION OF NOVEL MOLECULES IN THE SPECTRUM OF 19 PISCIUM

ROBERT S. WOJSLAW AND BENJAMIN F. PEERY, JR.
Department of Astronomy, Indiana University

Because of their severe violet deficiencies, spectra of stars of type N heretofore have not been analyzed in detail in wavelengths much shortward of Hγ. A Mount Wilson coudé spectrogram of 19 Psc (N0; C7, 3) at 1 nm mm^{-1} has recently been analyzed between λ398 nm and λ434 nm (results to be published by Peery).

In this spectral interval a number of absorption features of weak or moderate strength have resisted identification with conventional atomic and molecular sources. We suggest here the identification of 230 violet absorption features with 379 lines of electronic transitions out of the ground electronic states of CuH, ZnH, GeH, and SnH. Identifications are based upon (i) coincidences with published laboratory wavelengths, and (ii) the peculiar pattern of relative line strengths that characterizes each of the hydrides. Approximately one-quarter of these 230 stellar absorption features do not submit to plausible alternative identification; the remainder are blends of our proposed molecular lines with lines of conventional atoms and molecules.

In the stellar spectrum the (0, 0) band of the resonance electronic transition of CuH shows the peculiarity of breaking off at approximately $J'' = 6$. Laboratory studies reveal the character of this band to be governed by the *total* gas pressure (not simply the partial pressures of H and Cu): the greater the gas pressure, the larger the number of lines that appear in the (0, 0) band. In the laboratory the band breaks off at $J'' = 6$ when $\log P_{\rm gas} \approx 2$. This is the order of magnitude of the effective atmospheric pressure of a cool supergiant with $\log g \approx 0$.

The strengths of the proposed absorption lines of GeH and SnH relative to those of SiH lead us to conclude that the abundances of Ge and Sn are enhanced by 10–100 times as a consequence of *s* processing within the star.

INFRARED PHOTOMETRY OF RT LACERTAE

E. F. MILONE
The University of Calgary

The first of a number of eclipsing binaries with asymmetric light curves has been examined in the near-infrared for evidence of a distribution of matter in and around the Roche lobes.

The double-lined spectroscopic and peculiar eclipsing binary RT Lacertae has an apparent excess of radiation at *JHKL* over what is to be expected of the component stars, with due allowances for a reasonable degree of interstellar extinction, for "reflection" effects, and for the shape distortions and light distributions across the stellar faces. The peak value reached is about 0.7 mag at *K*. The excess has a phase-dependent component which reaches maximum, in the 1972–1974 light curves, near the secondary minimum and has an amplitude of about 0.3 mag at *K*. This component may be due either to reradiation effects from an envelope around the primary star or to infrared-radiating material concentrated near the outer Lagrangian point L_2. The remainder may be attributable to an anomalously high interstellar extinction resulting, perhaps, from mass loss from the system through L_2.

SYNTHESIS OF THE LIGHT ELEMENTS IN SUPERNOVAE

RICHARD I. EPSTEIN
Center for Astrophysics, Harvard College Observatory and Smithsonian Astrophysical Observatory
W. DAVID ARNETT*
Department of Astronomy, University of Illinois, Champaign-Urbana
AND
DAVID N. SCHRAMM
Enrico Fermi Institute, University of Chicago

The results of detailed calculations of possible nucleosynthesis in supernova shocks are presented. The shock waves are parametrized in such a way as to cover a wide variety of theoretical possibilities. Only if a strong high ion-temperature precursor develops does any appreciable nucleosynthesis occur. For presupernova stars with a Population I composition in their hydrogen-rich regions, only ^{7}Li and ^{11}B can be produced by the shock in interesting amounts; these isotopes are not efficiently produced by the interaction of galactic cosmic rays with the interstellar medium. If the hydrogen-rich region contains no CNO nuclei (as might be the case in an extreme Population II object), then ^{7}Li and possibly some deuterium could be produced. However, significant deuterium production requires extreme physical and astronomical conditions: (*a*) the ion precursor would have to develop only when the shock energy exceeds 40 MeV nucleon^{-1}; (*b*) the total energy of the supernova would have to be greater than $2 \times 10^{52}\ M_{SN}/M_\odot$ erg, where M_{SN} is the mass of ejected material. The restrictions on deuterium production would be eased somewhat if the ion precursor were stronger than Colgate found; however, the calculations of Weaver and Chapline may indicate that the precursor is actually less intense.

SPECTROSCOPY OF 206 QSO CANDIDATES AND RADIO GALAXIES

D. WILLS AND BEVERLEY J. WILLS
McDonald Observatory and University of Texas Radio Astronomy Observatory

We present the results of spectroscopic observations of 206 faint objects. The largest group consists of 113 radio-source identifications based on accurate (1″–2″) radio positions measured at the University of Texas Radio Astronomy Observatory (UTRAO), combined with optical positions accurate to 0″.5 measured from the *National Geographic Society–Palomar Observatory Sky Survey* plates. Of the remaining 93 objects, 72 come from other lists of suggested radio-source identifications and 21 are from lists of optically selected "radio-quiet" QSOs with ultraviolet excess. Of the 206 objects, 95 are definitely QSOs, nine have apparently continuous spectra (and are probably QSOs or related objects), 14 are galaxies (most with emission-line spectra), and 46 are galactic stars presumably unrelated to the radio sources. Results for the remaining 42 objects are not conclusive, although 20 of them are probably QSOs and a further 10 are probably stars. Descriptions of the spectrograms are given, together with other information on the radio and optical objects. The objects are then discussed in several subsets, the largest being the UTRAO identifications.

Combining the present results with those in an earlier paper, we present a table summarizing the spectroscopic results for 154 apparently stellar identifications (blue, red, or neutral) based on UTRAO positions. Spectroscopy of 60 blue stellar objects (BSOs) found within 3″ of UTRAO positions shows 49 of them to be definitely QSOs. Of the remainder, classed as inconclusive, eight are probably QSOs, based on the ultraviolet continuum, the existence of a probable emission line, or lack of stellar absorption lines in a well-exposed spectrogram. The remaining three objects could not be classified. We have not yet found a definite case of a star among these 60 BSOs within 3″ of the UTRAO positions, which confirms our earlier estimates of the reliability of the UTRAO identifications. Extending the sample to include 87 BSOs out to 5″ from the radio positions, we find 70 definite QSOs, 12 probable QSOs, three inconclusive objects, and only two definite stars. Among the 27 BSOs in the interval 5″–10″ from the UTRAO positions, 11 to 12 are QSOs and 12 to 15 are stars. These comparatively large radio-optical position differences arise because of unusually large radio position uncertainties or because of the angular structure of the radio source, which causes the radio and optical centroids to differ significantly. In support of the latter suggestion, we find the QSOs this far from the radio positions to have systematically smaller redshifts than do the objects closer to the UTRAO positions, although some of this effect is due to our restriction to observations of the optically brighter QSO candidates at this distance from the radio positions.

Other objects discussed include the neutral stellar objects found by Browne, Crowther, and Adgie (1973), some of which were found independently as UTRAO identifications. We also observed six of Braccesi's optically selected QSO candidates; three were found to be white dwarf stars (AB 28, 99, 159), two are probably QSOs (AB 55, 118), and one (AB 46) has an apparently continuous spectrum; four-color photometry of the latter by T. D. Kinman strongly suggests that it is a hot subdwarf. Of five objects from Weistrop's (1973) list of faint blue stars, selected as good QSO candidates, all were found to be QSOs. Observations of six of the identifications of Bologna radio sources with optically bright objects suggested by Battistini, Braccesi, and Formiggini (1974) show them all to be QSOs, making their total of 11 objects all reliable identifications. We found one QSO in the most recent Markarian list (Mkn 679), while two others in the list (Mkn 677, 690) are stars, without ultraviolet excess.

The Appendix to the paper lists optical positions for 66 of the objects discussed; they were measured from the Sky Survey plates and have rms uncertainties of about 0″.5.

REFERENCES

Battistini, P., Braccesi, A., and Formiggini, L. 1974, *Astr. and Ap.*, **35**, 93.
Browne, I. W. A., Crowther, J. H., and Adgie, R. L. 1973, *Nature Phys. Sci.*, **244**, 148.
Weistrop, D. 1973, *Astr. and Ap.*, **23**, 215.

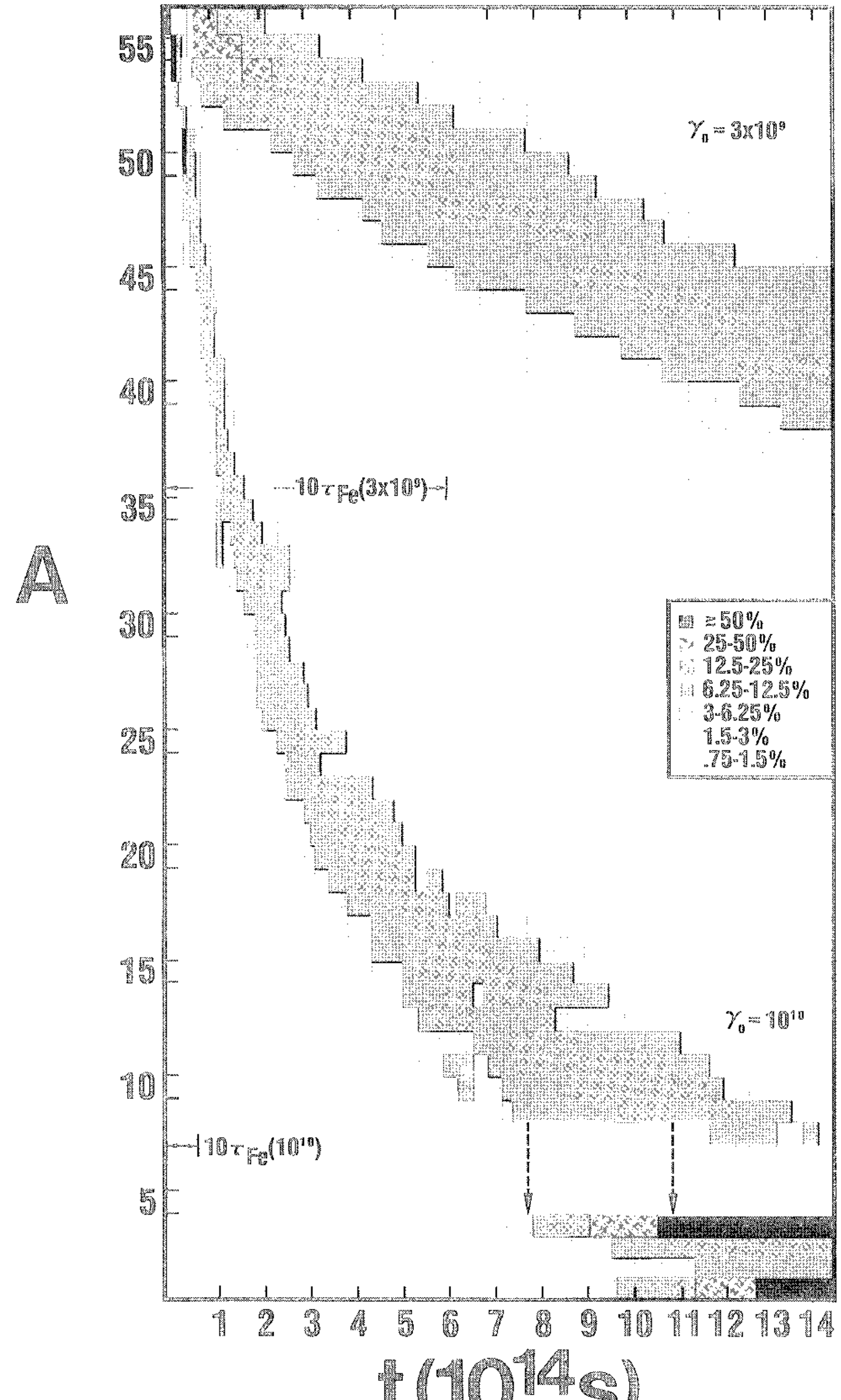

FIG. 9.—Calculated histories of two beams of ^{56}Fe nuclei with two different initial energies shown for the HIR case. Also shown in both cases are 10 times the value of the lifetime for Fe against one nucleon loss. The gap in the distribution for A between 4 and 9 is caused by the reaction $\gamma + {}^9\text{Be} \rightarrow 2\alpha + n$. The intensities shown for $A = 1$ and 4 are underestimated, since they do not include the contribution of the secondary products of the photoemission interactions.

PUGET *et al.* (*see* page 649)